Received: 4 February 2021 | Revised: 27 April 2021 | Accepted: 2 May 2021

DOI: 10.1002/pro.4102

FULL-LENGTH PAPER

THE PROTEIN SOCIETY WILEY

Elucidation and control of low and high active populations of alkaline phosphatase molecules for quantitative digital bioassay

Hiroshi Ueno | **Makoto Kato** | **Yoshihiro Minagawa** | **Yushi Hirose** | **Hiroyuki Noji**

Department of Applied Chemistry, Graduate School of Engineering, The University of Tokyo, Tokyo, Japan

Correspondence
Hiroyuki Noji, Department of Applied Chemistry, Graduate School of Engineering, The University of Tokyo, 7-3-1 Hongo, Bunkyo-ku, Tokyo 113-8656, Japan.
Email: hnoji@g.ecc.u-tokyo.ac.jp

Funding information
ImPACT Program of Council for Science, Technology, and Innovation, Japan Science and Technology Agency; Grant-in-Aid for Scientific Research on Innovation Areas from the Japan Society for the Promotion of Science, Grant/Award Numbers: JP18H04817, JP19H05380; Platform Project for Supporting Drug Discovery and Life Science Research (Basis for Supporting Innovative Drug Discovery and Life Science Research) from AMED, Grant/Award Number: JP21am0101115

Abstract

Alkaline phosphatase (ALP), a homo-dimeric enzyme has been widely used in various bioassays as disease markers and enzyme probes. Recent advancements of digital bioassay revolutionized ALP-based diagnostic assays as seen in rapid growth of digital ELISA and the emerging multiplex profiling of single-molecule ALP isomers. However, the intrinsic heterogeneity found among ALP molecules hampers the ALP-based quantitative digital bioassays. This study aims quantitative analysis of single-molecule activities of ALP from *Escherichia coli* and reveals the static heterogeneity in catalytic activity of ALP with two distinct populations: half-active and fully-active portions. Digital assays with serial buffer exchange uncovered single-molecule Michaelis–Menten kinetics of ALP; half-active molecules have halved values of the catalytic turnover rate, k_{cat}, and the rate constant of productive binding, k_{on}, of the fully active molecules. These findings suggest that half-active ALP molecules are heterogenic dimers composed of inactive and active monomer units, while fully active ALP molecules comprise two active units. Static heterogeneity was also observed for ALP with other origins: calf intestine or shrimp, showing how the findings can be generalized across species. Cell-free expression of ALP with disulfide bond enhancer and spiked zinc ion resulted in homogenous population of ALP of full activity, implying that inactive monomer units of ALP are deficient in correct disulfide bond formation and zinc ion coordination. These findings provide basis for further study on molecular mechanism and biogenesis of ALP, and also offer the way to prepare homogenous and active populations of ALP for highly quantitative and sensitive bioassays with ALP.

KEYWORDS
alkaline phosphatase, cell-free protein synthesis, digital bioassay, microdevice, protein maturation, single enzyme activity

Hiroshi Ueno and Makoto Kato contributed equally to this study.

1 | INTRODUCTION

Digital bioassays are an emerging bioanalytical strategy for highly sensitive, quantitative analysis of biomolecules, with single-molecule detection sensitivity.[1,2] In typical digital bioassays, the reaction mixture is partitioned into massive number of small reaction compartments, so that a single target molecule is stochastically encapsulated into a compartment. As a result, each compartment contains either no molecules or single target molecules. When a target molecule starts or triggers the fluorogenic reaction, compartments that contain a target molecule glow brightly due to accumulated fluorescence dyes, while empty compartments remain dark. Thus, by binarizing each fluorescent signal into "1 (positive)" or "0 (negative)", the number of target molecules can be determined as the number of positive compartments. The size reduction of the compartment is one of the critical features for establishing digital bioassays. This is because smaller reactors generally give higher signal-to-background ratios. Large-scale integration of micro-reactors is another key feature of digital bioassays, which can be used to achieve high sensitivities and wide dynamic ranges.[2]

To date, various types of digital bioassays have been developed. One example is a digital polymerase chain reaction (digital PCR) that partitions sample mixtures into many reactors and conducts PCR from single molecules of target DNA. Due to the exponential nature of the amplification reaction, digital PCR can be achieved by using conventional multi-well plates or test tubes, as demonstrated in the late 1990s.[3] Microfluidic methods to produce considerable micro-reactors or water-in-oil emulsions allow for more prompt and high-throughput digital PCR.[4–8]

Another representative bioassay is digital enzyme-linked immunosorbent assay (digital ELISA).[9,10] Due to its highly quantitative nature, and its ultra-high sensitivity that often extends toward sub-femtomolar, digital ELISA is expected to be one of the standard platforms for next-generation diagnostic testing. In the typical form of digital ELISA, fluorescence signal is generated from antibody-conjugated enzyme that conducts fluorogenic reaction, although enzyme-free systems were reported recently.[11,12] Unlike PCR, the signal of a fluorogenic assay linearly increases with time. Therefore, digital enzyme bioassays have had to wait for micro-compartment technology that enables partitioning of solution into extremely small reactors with volume of femotoliters to emerge. In early digital enzyme bioassays, polydimethylsiloxane or glass fiber-based reactor devices were used.[13] In recent reports, various formats for micro-compartmentalization have been used: water-in-oil (w/o) droplet arrays,[14] freely suspended w/o droplets,[15] or slip chips,[16] uniform femto-liposome,[17] and so forth. Along with the development of micro-compartmentalization technology, various types of digital bioassays have been reported for enzymes, for example, β-galactosidase,[18–20] β-glucuronidase,[21] horseradish peroxidase,[19,22] alkaline phosphatase (ALP),[23] and influenza viruses,[24,25] and also for membrane transporters,[17,26] and cell-free gene expression.[17,27]

ALP, a ubiquitous enzyme found in many species, is a metalloenzyme that catalyzes the hydrolysis of phosphate monoesters under basic pH conditions. Most of the ALP enzymes, including those from *Escherichia coli*, calf intestines and shrimp, forms a homodimer with two catalytic sites on each monomer unit.[28] ALP is widely used as a label enzyme in many bioassays, including in ELISA assays, due to its high catalytic turnover rate (100–1000 turnover/s) that gives it a high signal-to-noise ratio. Therefore, there is a large demand for creating an ALP-based digital ELISA that would facilitate the digitalization of many already developed conventional ELISAs. Additionally, certain human ALPs types are widely used as biomarkers in diagnostic tests, such as for bone diseases and human cancers.[29–34] Recently, we developed a multiplexed single-molecule enzyme assay for counting disease-related human ALP isoforms.[35] Another analysis on human ALP isoforms with digital assay showed that some of tissue-specific isoforms have distinctive activity distributions of single enzymes,[36] suggesting the possibility to detect disease specific signal that is masked in ensemble averaging in conventional ALP assays. Thus, digital ALP bioassays and related enzymes hold great potential for not only expanding digital ELISA assays, but also for novel multiplexed enzyme profiling for detecting diseases.

However, through the digital bioassays of ALP, it is well recognized that ALP enzymes have intrinsic heterogeneity in catalytic activity distribution.[35–38] The heterogeneity principally hampers the digital bioassay based on binarization of enzyme activity. It also makes single-molecule multiplex profiling difficult. In order to settle the heterogeneity of ALP enzymes, quantitative kinetic analysis of single ALP enzymes as well as the elucidation of biogenesis mechanism of the heterogeneity are required.

In this study, we conducted a quantitative single-molecule assay of ALP from *E. coli* (*Ec*ALP) as a model system of ALP by using a femtoliter reactor array device. We revealed that ALP has two distinctive elements: half-active and fully active molecules. We further investigated single-molecule Michaelis–Menten kinetics with serial buffer exchange system. We also analyzed ALP molecules synthesized in various gene expression conditions with a cell-free expression system. These experiments revealed the biogenesis mechanism behind static heterogeneity

giving two distinctive fractions, and also offered the way to prepare a homogeneous population of ALP molecule with full activity.

2 | RESULTS AND DISCUSSION

2.1 | Single-molecule analysis of *Ec*ALP

In this study, *E. coli* ALP (*Ec*ALP) was used as a model enzyme, unless stated otherwise (Figure 1(a)). After expression in *E. coli*, *Ec*ALP was purified as a recombinant enzyme with histidine-tag at the N-terminus (please see the experimental section for details). For single-molecule analysis, a solution of *Ec*ALP was diluted to 500 fM or less to ensure a "digital condition", where the mean number of *Ec*ALP molecules per reactor (λ) was well below 1. Thus, almost all the reactors should be empty, with only a few reactors containing a single-molecule of the *Ec*ALP enzyme. For quantitative measurement, a fluorogenic substrate, fluorescein diphosphate (FDP) was mixed with the enzyme solution at 1 mM. The reaction mixture was infused into a flow cell (Figure 1(b)) that was assembled from a top glass plate that contained both inlet and outlet holes, a spacer sheet, and a femtoliter reactor device that displayed over millions of reactors 3 and 4 μm in depth and diameter, respectively. Reactors were sealed with oil, and the flow cell was incubated on the microscope stage for time-lapse imaging at room temperature (23°C). Figure 1(c) shows the fluorescence images of the digital *Ec*ALP enzyme assay. Among the many dark reactors, a few bright reactors were observed. Dark reactors represented empty ones, while bright reactors contained reactors that encapsulated single molecules of *Ec*ALP. Note that the dark reactors also exhibited increased fluorescence signals slowly. This is due to the spontaneous hydrolysis (autolysis) of FDP.

2.2 | Static heterogeneity with two distinct populations

Figure 2(a) shows the typical time courses of fluorescence signals obtained at 50 fM [*Ec*ALP]. The fluorescence intensity increased linearly with time. The time courses showed two

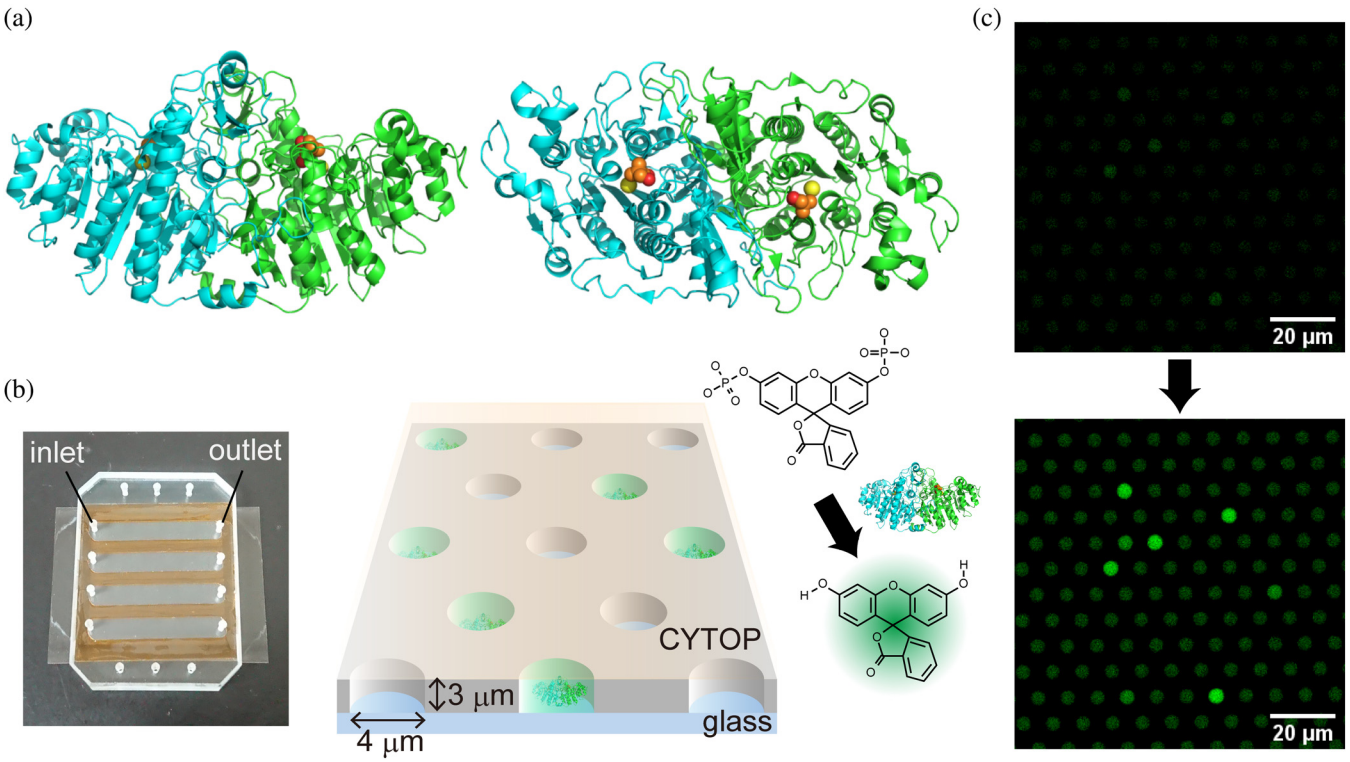

FIGURE 1 Single-molecule assay of ALP with femtoliter droplet array. (a) Homo-dimeric structure of ALP (side and top views). The red, yellow, and orange spheres show Zn^{2+}, Mg^{2+}, and inorganic phosphate, respectively, (b) photo of a flow cell and schematic of the femtoliter droplet array. This device has 6×10^6 uniform microwells (4 μm in diameter and 3 μm in height) on a glass surface. Reactors are covered with oil to seal and encapsulate the enzyme molecule with a fluorogenic substrate, FDP. Non-fluorescent FDP was hydrolyzed into a highly fluorescence dye, fluorescein, by ALP. Finally, (c) time-lapse fluorescence images of a digital enzyme assay of wild-type *Ec*ALP purified from *Escherichia coli* after 60 min (top) and 360 min (bottom)

distinctive populations: low-activity (*L*) and high-activity (*H*) ones, in addition to the majority of empty reactors (ϕ).

The histogram of the reaction rate (slope) shows that the activity of the low-activity group was approximately 50% of that of the high-activity group (Figure 2(b)). One may consider that the high-activity group represents the activity of two molecules of the enzyme. However, both of the low-activity and high-activity reactors should correspond to reactors containing a single-molecule of *Ec*ALP, while taking into account that λ is well below 1. Thus, the probability to encapsulate two or more molecules in a reactor, $P(n \geq 2)$, should be significantly lower. To verify this contention in a more quantitative manner, we conducted a statistical analysis of the data obtained at different *Ec*ALP concentrations: 5, 50, and 500 fM. Low-activity and high-activity reactors always appeared as two distinct peaks in the activity histograms (see insets of Figure 2(b,c)). The majority of empty reactors were located at the leftmost peaks. For the quantitative estimation of $P(n \geq 2)$, λ values were determined from the probability of positive reactors with a bright fluorescence signal; $P_{\text{positive}} \equiv P(n \geq 1)$, according to the following equation[2]: $\lambda = -\ln(1 - P_{\text{positive}})$.

The experimentally determined λ values were 4.4×10^{-3}, 3.0×10^{-2}, 3.2×10^{-1} for 5, 50, and 500 fM of [*Ec*ALP]s, respectively (Figure 2(d)). The probability of encapsulation of two or more molecules, $P(n \geq 2)$, was then estimated to be 9.7×10^{-6}, 4.4×10^{-4}, 4.1×10^{-2} for 5, 50, and 500 fM of [*Ec*ALP]s. These values were 0.22, 1.5, and 15% of P_{positive} at 5, 50, and 500 fM [*Ec*ALP]s. Thus, the ratio of the high-activity reactor should be dependent on [*Ec*ALP]s if the high-activity represents the activity of two or more molecules of *Ec*ALP. On the other hand, the experimentally observed proportion of high-activity reactors was consistently approximately 40%–50% at all [*Ec*ALP]s (Figure 2(e)). These findings mean that both the low-activity and high-activity reactors correspond to reactors containing only single molecules of

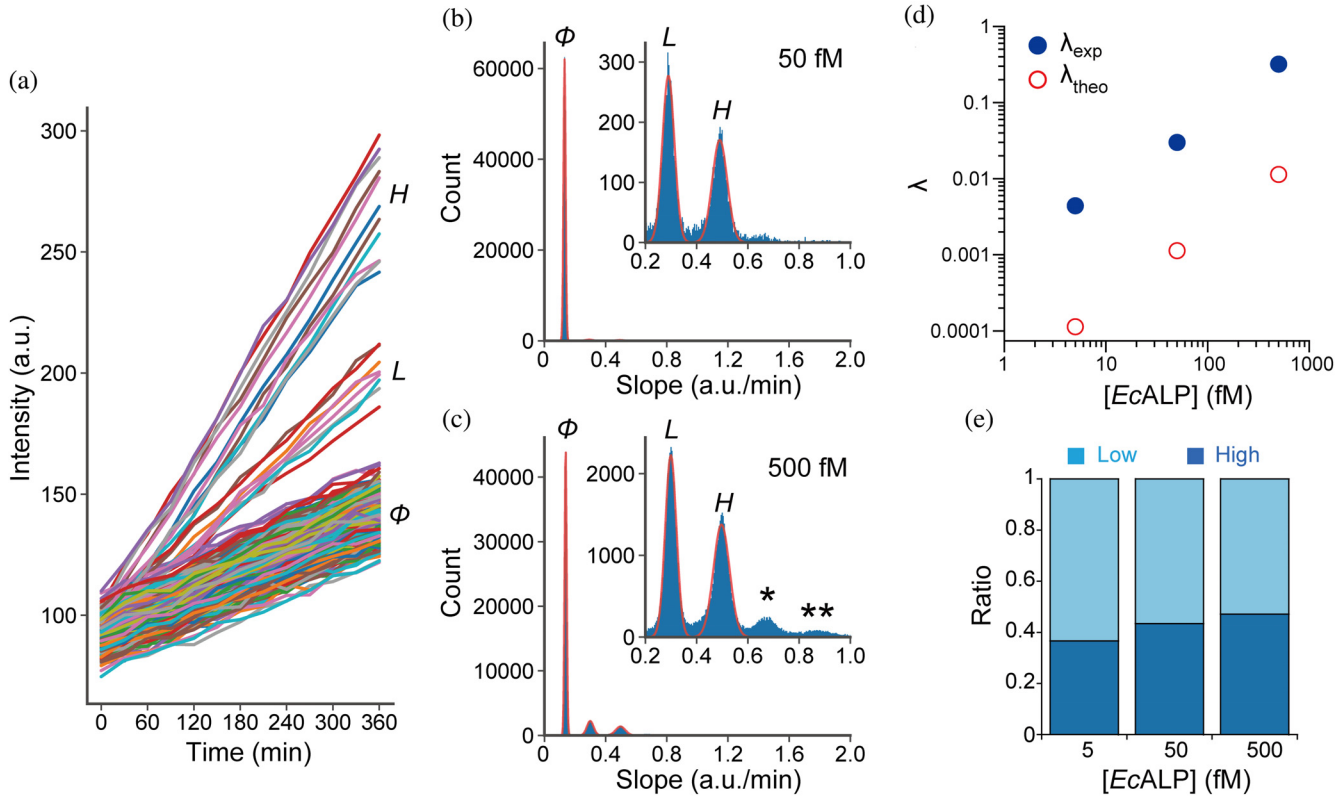

FIGURE 2 Two distinct populations of single-molecule activity of *Ec*ALP. (a) Typical time courses of fluorescent intensity of the reactors at 1 mM FDP and at 50 fM [*Ec*ALP]. Symbols ϕ, *L*, and *H*, represent the main empty reactors, the low-activity group, and the high-activity group. (b, c) Show a histogram of catalytic activity (slope = fluorescence increment over time) of the reactors at 50 fM (b) and 500 fM [*Ec*ALP] (c). A single asterisk and double asterisk in the inset of (c) represent the reactors putatively containing two molecules of *Ec*ALP; low-activity and high-activity molecules (single asterisk), or two molecules of the high-activity group (double asterisk). (d) Shows the experimentally determined (blue circles) and theoretically calculated (red circles) number of positive reactors per reactor (λ) versus [*Ec*ALP]. The threshold for the positive reactors is 0.2 (a.u./min), and (e) shows the ratio of low- or high-activity group against the sum of low- and high-activity groups. Wild-type *Ec*ALP purified from *Escherichia coli* was used in this experiment. Time-lapse images were obtained at 30 min intervals for a total of 360 min

*Ec*ALP. One may still consider the possibility to encapsulate two enzymes in a reactor, by assuming that intermolecular dimer or oligomer formation between/among ALP molecules cross-linked by occasional disulfide bonding of cysteine residues. However, SDS-PAGE analysis under non-reducing conditions excluded such possibilities (Figure S1).

Notice that two very small portions at right side of high-activity were found at 500 fM (single or double asterisks in the inset of Figure 2(c)). These correspond to the reactors containing two molecules of the enzyme: a pair of low-activity and high-activity molecules for the single asterisk and two molecules of the high-activity group with a double asterisk. Also, it should be noted that the experimentally determined λ was ∼30 times higher than the theoretical value that was calculated from the reactor volume and [*Ec*ALP] (Figure 2(d)). This may be because the histidine-tagged *Ec*ALP molecules preferentially attach to the bottom glass surface of the reactors via non-specific absorption of his-tag as seen in other single-molecule studies.[39,40] The attachment of *Ec*ALP was confirmed in the serial buffer exchange experiment (see below).

2.3 | Heterogeneity found in other ALPs

To investigate the generality of ALP static heterogeneity, we examined the single-molecule activity of commercially available *Ec*ALPs and ALPs from different species (Figure 3(a-d)). All of the tested ALPs were analyzed at $\lambda = 0.03$, where the probability of encapsulation of two or more molecules was negligible.

*Ec*ALP (TOYOBO), calf intestinal ALP (Roche), and shrimp ALP (TaKaRa) showed clear static heterogeneity. *Ec*ALP from TOYOBO and Shrimp ALP exhibited two forms: a low-activity group and a high-activity group, of which the activity exhibited a 1:2 ratio similar to the recombinant *Ec*ALP. Calf intestine ALP showed triplet peaks. The low- and middle-active groups have activities with a 1:2 ratio in similar to other ALPs. Although the exact origin of the third peak is unclear, a post-translational modification, such as proteolytic processing and glycosylation, could cause additional static heterogeneity.

These findings indicate that static heterogeneity is a common feature that was conserved from prokaryotes to eukaryotes. Among the ALP's tested, only *Ec*ALP (TaKaRa) showed no obvious peaks in the histogram, which implies that static heterogeneity originates from differences in gene expression, or purification procedure. In the last part of this study, we show that the gene expression condition is the critical factor for static heterogeneity.

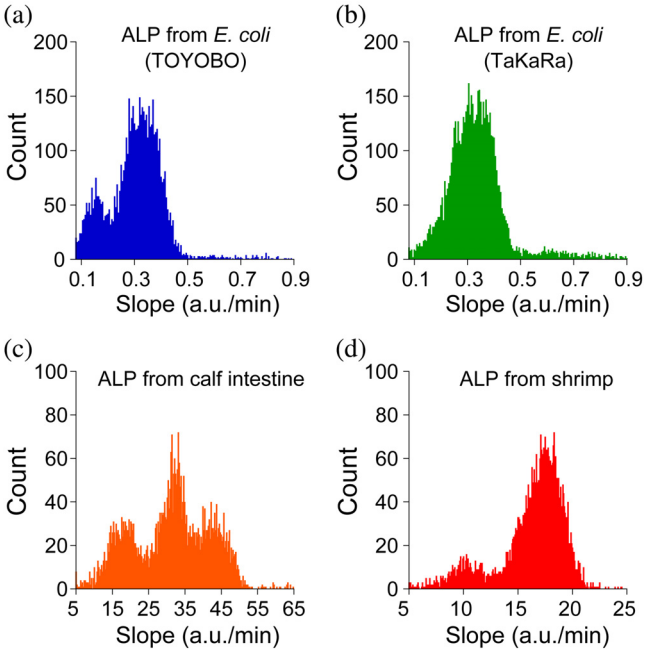

FIGURE 3 Histograms of single molecule activity of ALPs from (a) *Escherichia coli* (TOYOBO), (b) *E. coli* (TaKaRa), (c) calf intestine (Roche), (d) and shrimp (TaKaRa). The peaks of the empty reactors (background) were omitted for clarity. Time-lapse images were obtained at 20 min intervals for a total of 360 min

2.4 | Michaelis–Menten analysis for single ALP molecules

To further characterize the two populations found in the ALP: low-activity and high-activity groups, we performed single-molecule Michaelis–Menten kinetics analysis by changing the substrate concentrations in the reactors (Figure 4(a)). In this experiment, we used a highly active mutant *Ec*ALP (D101S),[41] which also exhibited clear static heterogeneity with low-activity (50% active) and high-activity (100% active) groups, identical to the wild-type *Ec*ALP. The high catalytic activity of the mutant allows for quantitative measurements even under substrate-limiting conditions ($\ll K_m$) where the catalytic activity is significantly low. Figure 4(a) (left) shows a schematic image of the successive serial buffer exchange process in which the ALP molecules were retained in the reactors via the abovementioned non-specific absorption through his-tag. In this way, the catalytic activity of individual enzyme molecules was measured at different concentrations of the substrate (FDP) for single-molecule Michaelis–Menten analysis.

The fluorescence images of catalytic activity measured at 30, 100, and 300 μM FDP were shown in Figure 4(a) (right). We observed that the catalytic activity of the enzyme molecules increased as the substrate concentrations increased. By fitting the data points from

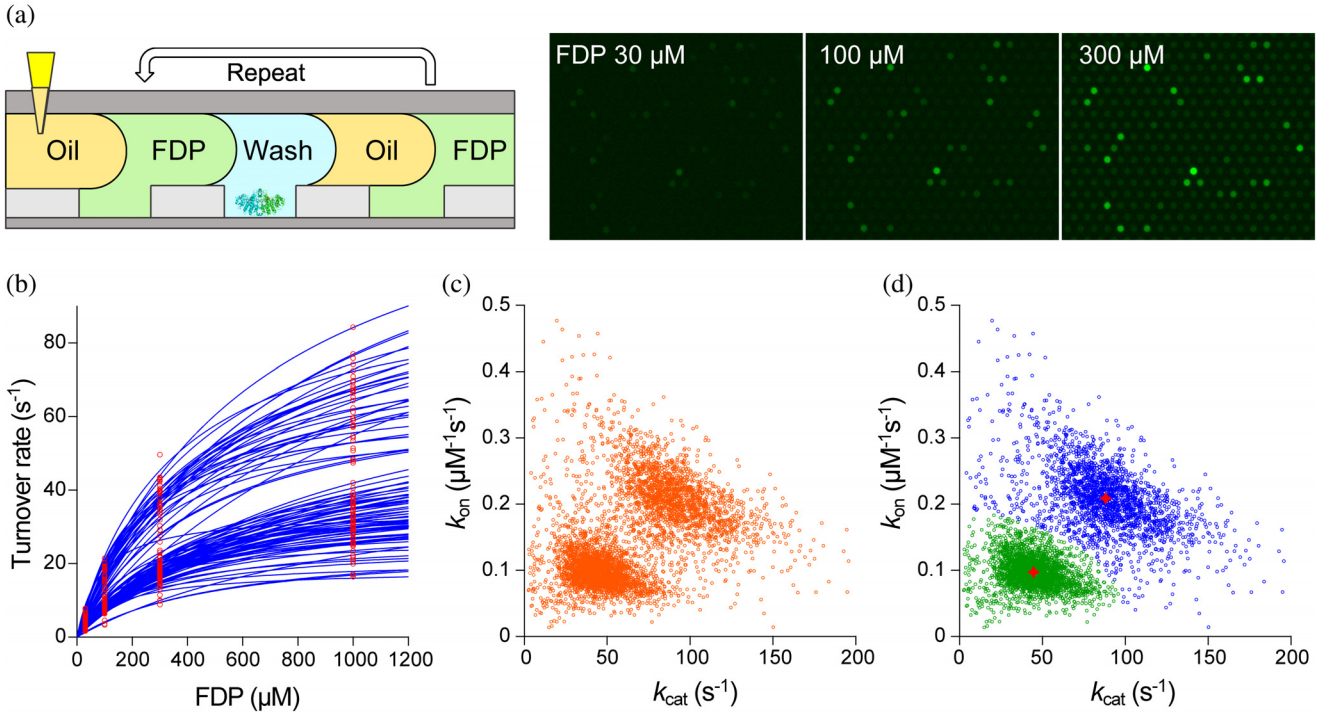

FIGURE 4 Single-molecule Michaelis–Menten analysis of *Ec*ALP (D101S). (a) shows a schematic of the successive serial buffer exchange for digital bioassays at different substrate (FDP) concentrations. The right images show the fluorescence images after 40 min incubation obtained at 30, 100, and 300 μM FDP. (b) shows the typical Michaelis–Menten kinetics of the single-molecule ALP molecules (randomly sampled 100 molecules). Red dots represent the turnover rates obtained at indicated concentrations of FDP. The turnover rates were calculated as rates of one dimer in each reactor, and (c) depicts the two-dimensional plot of k_{cat} and the rate constant of productive binding: $k_{cat}/K_m = (k_{on})$ determined from Michaelis–Menten analysis in (b). Orange circles represent data points ($n = 5014$) obtained by serial buffer exchange assays. Finally, (d) shows the clustering analysis for all data sets from (c). The green and blue circles are identified as clusters by Gaussian Mixture Model clustering. The mean values (red stars) of k_{on} and k_{cat} for each cluster were 0.097 μM^{-1} s^{-1} (green: low-activity), 0.21 μM^{-1} s^{-1} (blue: high-activity) and 45 s^{-1} (green: low-activity), 88 s^{-1} (blue: high-activity), respectively. *Ec*ALP D101S mutant purified from *Escherichia coli* was used in this experiment. Time-lapse images were obtained at 10 min intervals for a total of 40 min

each molecule with the Michaelis–Menten equation, K_m and k_{cat} were determined for each molecule (Figure 4(b)). The rate constant of the productive substrate binding, k_{on} was then determined as k_{cat}/K_m. The plot of k_{on} versus k_{cat} (Figure 4(c)) clearly shows two distinctive groups. Figure 4(d) shows the cluster analysis of all the data points that identified the two groups that correspond to low-activity (green) and high-activity (blue) groups. The average values of k_{on} and k_{cat} for each group was determined to be 0.097 μM^{-1} s^{-1} and 45 s^{-1} for the low-activity group, and 0.21 μM^{-1} s^{-1} and 88 s^{-1} for the high-activity group, respectively. Thus, single-molecule Michaelis–Menten analysis revealed that the kinetic parameters of the low-activity group were approximately 50% of the high-activity group. Considering the homo-dimeric structure of ALP, the simplest explanation for the observed heterogeneity is that heterogeneity originated from the heterogenic dimerization of ALP; low-activity molecules are composed of a fully inactive monomer and fully active monomer, while high-activity molecules are composed of two fully active monomers.

Interestingly, each cluster showed significant molecule-to-molecule distribution as shown as wide dispersion of points. Although this should include systematic experimental error to some extent (usually around 10%), this indicates molecule-to-molecule variations in kinetic parameters. Considering the kinetic parameters were determined from time-averaged measurement, this heterogeneity within the clusters implies the existence of static conformational heterogeneity within low-active or high-active population.[21]

2.5 | Effect of post-translational maturation on heterogeneity

*Ec*ALP requires the coordination of one Mg^{2+} and two Zn^{2+} ions per monomer for catalysis.[42,43] Some reports have suggested that Zn^{2+} coordination is also important

for the maintenance of dimeric quaternary structure of ALP.[44,45] In addition, each monomer of *Ec*ALP has two disulfide bond pairs, Cys^{168}-Cys^{178} and Cys^{286}-Cys^{336}. The latter pair was reported to be crucial for catalysis.[46] Based on these previous biochemical studies, we hypothesize that the deficiency in correct disulfide bond formation and/or metal incorporation in the post-translational process result in the inactive monomer, yielding the static formation of heterogenic dimers.

To test this idea, we assayed *Ec*ALP that was expressed in the presence of a disulfide bond enhancer (PDBE)[47] and/or excessive amounts of Zn^{2+} ions. Recombinant wild-type *Ec*ALP was prepared in cell-free gene expression by using a mixture of protein synthesis with recombinant elements[48] (PURExpress; New England Biolabs) with PDBE and/or $ZnSO_4$. Then, the resulting *Ec*ALP molecules were assayed. Figure 5(a) shows the histograms obtained with or without PDBE and/or $ZnSO_4$. When either PDBE and $ZnSO_4$ was added into the cell-free expression mixture, the expressed ALP exhibited slightly improved heterogeneity, and the high-activity group was more abundant. When both PDBE and $ZnSO_4$ were added, heterogeneity almost disappeared, thus showing a single fraction of the high-activity group (Figure 5(a,b)). These results provide important implications about functionalization of ALP. First, it is highly likely that the static heterogeneity of ALP is due to a defect or an error in disulfide bond formation and Zn^{2+} incorporation. When combining with the idea on the heterodimer, this means that the inactive monomer is deficient in correct disulfide bond formation or Zn^{2+} incorporation. Another implication is that both of correct disulfide bond formation and Zn^{2+} incorporation are requisite for gaining the catalytic activity of monomers; otherwise, monomer remains almost fully inactive. This contention is supported by previous biochemical studies.[46,49–51]

We also tested the possibility of improving heterogeneity by soaking expressed *Ec*ALP protein in $ZnSO_4$ buffer, with the expectation of incorporating Zn^{2+} ions after the dimeric assembly formation of ALP. However, post-synthesis soaking of ALP, which was prepared by the cell-free protein synthesis with PDBE, in the Zn^{2+} buffer did not improve heterogeneity (Figure S2). This means that Zn^{2+} ions can be efficiently incorporated into ALP when ALP is in the folding or maturation process.

It should be noted that a variety of studies have reported the presence of isozymes of *Ec*ALP that have different N-terminal residues, which are generated by post-translational processing, after removal of a signal peptide, during maturation.[52–55] These studies employed signal peptides for the secretion of ALPs into periplasm space

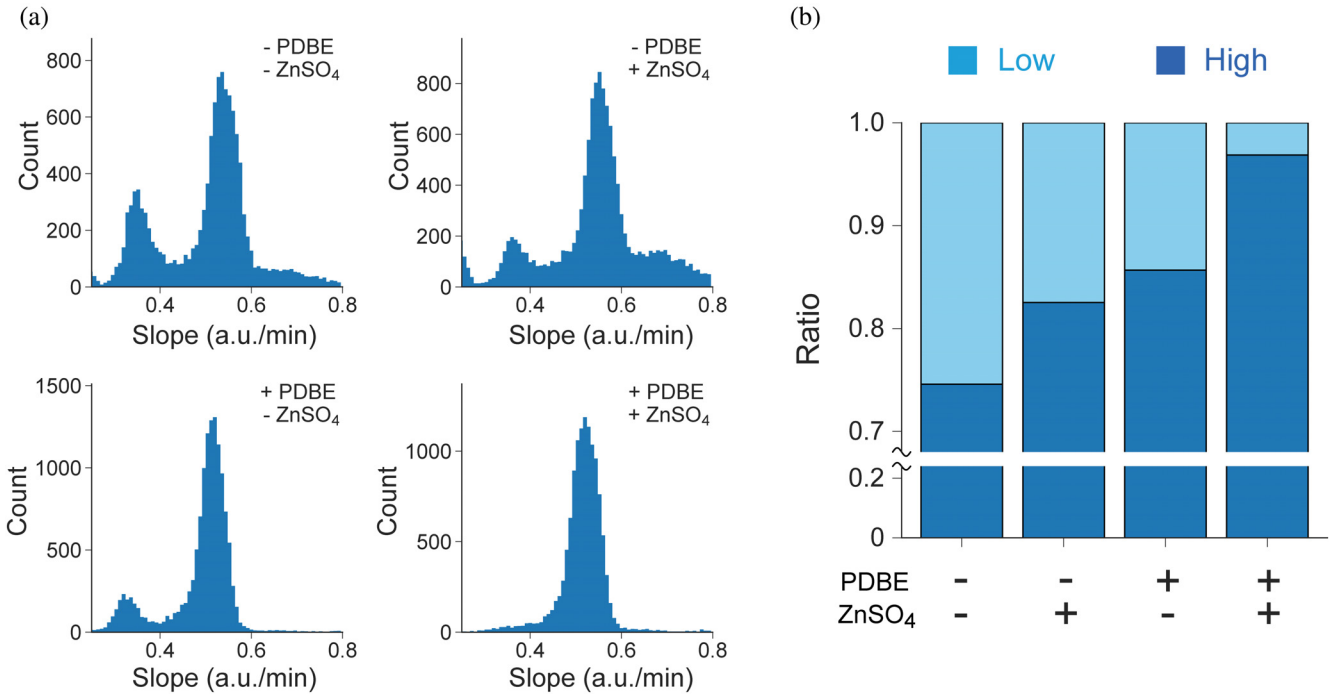

FIGURE 5 The impact of disulfide bond enhancer (PDBE) and Zn^{2+} on single-molecule activity of ALP. (a) shows the histograms of single-molecule activity of ALP with or without PDBE and 100 μM $ZnSO_4$ at $\lambda = 0.05–0.06$ conditions, The final dilution factors of cell-free expressed ALP were 2×10^6 (upper left, upper right) and 2×10^7 (lower left, lower right), respectively, and (b) shows the ratio of low- or high-activity group against the sum of low- and high-activity groups observed in (a). Cell-free expressed wild-type *Ec*ALP was used in this experiment. Time-lapse images were obtained at 10 min intervals for a total of 360 min

where the disulfide bond formation in monomers is mediated with Dsb proteins under oxidative environments. On the other hand, in this study, the recombinant *Ec*ALP was expressed without signal peptide and purified with N-terminal histidine-tag. Therefore, the heterogeneity found in recombinant *Ec*ALP is not attributable to the heterogeneity of the post-translational truncation of the -N-terminal residues. In the case of *in-cell* expressed ALP's, it would be possible to have additional static heterogeneity due to post-translational modifications such a post-translational truncation or modification with polysaccharides,[37] as found in calf intestinal ALP (Figure 3(c)).

3 | CONCLUSIONS

In summary, the present single-molecule analysis on ALP revealed static heterogeneity hidden in average ensemble bulk measurements. The time-lapse and the histogram of single-molecule activity of *Ec*ALP showed two distinct populations: low-activity and high-activity groups for which the catalytic activities were found in a 1:2 ratio. Similar static heterogeneities were also found in other ALP enzymes from other species, suggesting the generality of static heterogeneity.

Single-molecule Michaelis–Menten kinetics analysis revealed that k_{on} and k_{cat} of the low-activity group were approximately 50% of those of the high-activity group. These findings suggest a simple mechanism for the static heterogeneity, that the half-active enzyme molecules are heterodimeric assembles of active and inactive monomers while high-activity molecules are homo-dimeric assemblies of active monomers. This idea implies that zero active homodimer complexes of inactive monomers would exist in the molecule population to some extent although the dimer forming efficiency between inactive monomer are unclear. More elaborated single-molecule analysis is required for the direct detection and quantification of zero active homodimers, for example, quantitative analysis of ALP molecules tagged with an optical marker such as nanoparticles or other enzymes.

Analysis of *Ec*ALP prepared in cell-free system suggests that the half-activity molecules are heterodimers with inactive monomer that is deficient in correct disulfide bond formation and/or Zn^{2+} incorporation.

This contention means that dimeric ALP has no or week catalytic cooperativity between the monomers under the current conditions. In other words, the activity of ALP can be expressed by 2-bit binary number with binary digits, "0 (inactive)" and "1 (active)" (Figure 6). This binary activity model is apparently inconsistent with an extreme version of allosteric model for ALP termed "half-of sites model", proposed in some early studies.[56–58] Half-of sites model assumes that catalytic activities on two monomer units are tightly coupled and that the catalytic/conformational states of monomers are reciprocally switched upon catalytic turnover.[56] Such tightly coupled models are contradicting to the binary activity model assuming independent catalysis on monomers. There are also some reports that suggest interplay between catalytic sites, based on the deviations of kinetic data points from simple kinetic models.[58,59] In the present experiments, signs of modest cooperativity might be masked in the molecule-to-molecule variations and experimental errors. More intensive analyses are required for assessment and elucidation of allostery of ALP. In addition, re-evaluation of previous kinetic studies could also give some new clues on molecular mechanisms of ALP, taking the static heterogeneity of ALP molecule into account. More experimental analysis is required to fully address the long-debated issue on allostery of ALP.[60–62]

4 | MATERIALS AND METHODS

4.1 | Materials

Fluorescein diphosphate (FDP) and fluorescein were purchased from AAT Bioquest and Wako Pure Chemical, respectively. AE3000 and SURFLON S-386 were purchased from AGC Seimi Chemical, and Fomblin Y-25

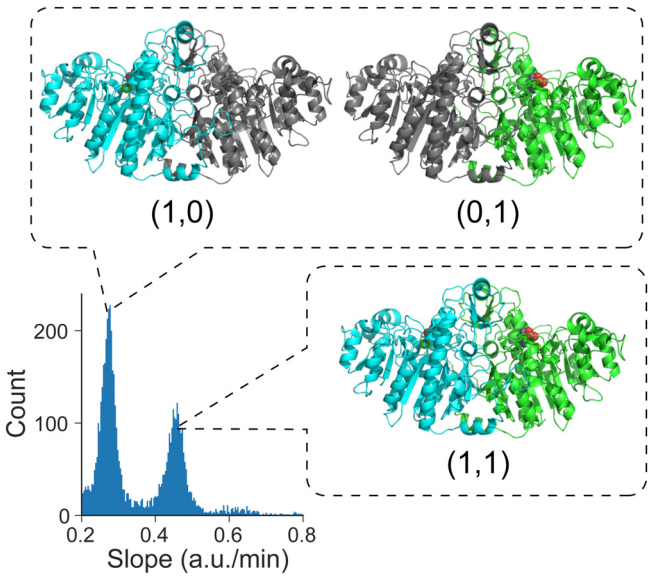

FIGURE 6 Proposed model for static heterogeneity of ALP. Active-inactive heterodimers correspond to low-activity molecules with 50% activity, where a homodimer from the two active monomers corresponds to high-activity molecules with 100% activity. Inactive monomers are deficient in correct disulfide bond formation and/or zinc ion incorporation

was purchased from Solvay. Mineral oil was purchased from Sigma-Aldrich. The PURExpress In Vitro Protein Synthesis Kit and disulfide bond enhancer (PDBE) were purchased from New England Biolabs, while CYTOP and AZ-4203 were purchased from AGC Chemicals and AZ Electronic Materials, respectively. AZ300MIF was purchased from Merck, and the commercial alkaline phosphatases (ALPs) derived from *E. coli* (TOYOBO or TaKaRa), calf intestine (Roche), and shrimp (TaKaRa) were purchased from their respective suppliers. Note that ALPs from TOYOBO and TaKaRa have no his-tag for purification.

4.2 | Fabrication of femtoliter droplet array device

A femtoliter droplet array was prepared by conventional photolithography technology,[27] as described below. An amorphous perfluoro polymer (CYTOP) was spin-coated on a glass coverslip ($24 \times 32\ mm^2$, Matsunami) and baked at 80°C for 10 min, followed by 180°C for 30 min. Afterwards, a positive photoresist (AZ-4203) was spin-coated on a CYTOP surface and baked at 100°C for 5 min. After exposure with a photomask, the photoresist layer was developed in a developer (AZ300MIF) for 90 s in a bath sonication device. The resist patterned CYTOP surface was dry-etched with O_2 plasma using a reactive ion etching system (RIE-10NR, Samco). The sample was then cleaned with acetone and isopropanol to remove the patterned photoresist layer completely. The resulting glass surface contained the CYTOP-patterned microwell array, which had a diameter of 4 μm and a height of 3 μm. The volume of one microwell was calculated to be ~40 fL. The patterned area was $20 \times 20\ mm^2$ and contained 6×10^6 uniform microwells. The flow channel was constructed by assembling the CYTOP-patterned glass coverslip, and the top glass contained the inlet and outlet ports, which were portioned with spacer tape (Teraoka).

4.3 | Preparation of ALP from *E. coli*

E. coli ALP (wild-type or D101S mutant) was expressed overnight at 37°C in *E. coli* C43 (DE3) cells, which harbored the pRSET-B plasmid coding for the ALP gene, where the His_6-tag, Xpress epitope, and enterokinase recognition sequences were inserted at the N-terminus of the ALP gene without a signal sequence. The enzyme was purified at 4°C through a nickel-nitrilotriacetic acid column (Ni-NTA superflow, Qiagen) using binding/wash buffer (50 mM Tris–HCl, pH 8.0, 100 mM KCl, 1 mM $MgCl_2$, 5 mM imidazole) and elution buffer (wash buffer supplemented with 500 mM imidazole), which was followed by a gel filtration column (Superdex 200, GE Healthcare) equilibrated with 20 mM Tris–HCl, pH 8.0, 100 mM KCl, 1 mM $MgCl_2$. We have not conducted post-expression processing to remove the his-tag. The concentration of proteins was determined by using the BCA protein assay kit (Pierce) with BSA as the standard. The purified protein was flash-frozen in liquid nitrogen and stored at −80°C.

4.4 | Cell-free ALP protein synthesis

ALP was synthesized using the PURExpress In Vitro Protein Synthesis Kit, as previously reported.[27] A reaction mixture containing 25 μl was incubated at 27°C for 4 h after the template DNA was added (5 nM) with or without the disulfide bond enhancer (PDBE) and 100 μM of $ZnSO_4$. PDBE is a mixture of proteins and buffers that can promote proper disulfide bond formation by assisting the oxidation of cysteines, as well as correcting incorrectly oxidized disulfides.[47] After the reaction, the resulting mixture was used for the ALP stock solution.

4.5 | Digital ALP enzyme assay

The ALP stock solution was diluted to the appropriate concentration (or the final dilution factor of 10^6–10^7 in the case of cell-free expressed stock solution) where the mean number of enzyme molecules per reactor (λ) was below 1 with the previously optimized assay buffer (1 M diethanolamine, pH 9.25, 1 mM $MgCl_2$, 0.02% Tween-20, 1 mM FDP),[23] after which the solution was infused into the array device. The assay buffer contained detergent that helps the homogeneous encapsulation of enzyme solution into the microwells. After chilling on ice to remove air from the microwells, the flush oil (AE3000 containing 0.1% SURFLON S-386) was injected to form the water-in-oil droplets. Following this, sealing oil (Fomblin) was infused to eliminate the evaporation of the aqueous phase. Within a few minutes after the dilution/encapsulation, time-lapse fluorescence images of the reactors were acquired using an epi-fluorescence microscope. In the case of serial buffer exchange experiment, mineral oil was used for flushing and sealing, and the wash buffer (assay buffer without FDP) was infused (~83 times the volumes of flow path) followed by infusion of indicated concentrations of FDP (~7 times the volumes of flow path) to serially exchange the substrate concentration. The single-molecule activity of ALP was measured from a time-lapse of the fluorescence intensity for each

reactor. A histogram of the fluorescence increase over time (slope) of the reactors shows a discrete peak that corresponds to the distribution of the activity of the enzyme that was encapsulated in the reactor. Based on the Poisson distribution where λ is much less than 1, a major peak in the histogram of slope should correspond to the background activities from the reactors that are encapsulating zero enzyme molecules. The second major peak should correspond to the activity of single enzyme molecule. The experimental λ_{exp} was determined from the number of bright reactors divided by the total number of observed reactors, with a threshold slope value for each experiment. The peak areas were determined using Gaussian fitting. The turnover rate was calculated as the rate of increase of fluorescein concentration per ALP dimer by using a calibration curve of fluorescein concentration versus fluorescence intensity. For Michaelis–Menten analysis, we omitted the data from the empty reactors and the reactors containing two or more ALPs by the threshold of mean fluorescence intensity of the major zero-peak (ϕ) and the high-activity peak (H) plus 4 × SDs, respectively. The clustering analysis of k_{on} and k_{cat} was performed by using a Gaussian mixture model implemented in Python with scikit-learn; https://scikit-learn.org/.[63] The data showing unusually high k_{on} (>0.5 μM^{-1} s^{-1}) and k_{cat} (>200 s^{-1}) were omitted from the clustering analysis. All assays were conducted at room temperature (23°C).

4.6 | Imaging and image analysis

Fluorescence images were acquired using an epi-fluorescence microscope (ECLIPSE Ti-E or Ti2, Nikon) equipped with a sCMOS camera (ORCA-flash 4.0, Hamamatsu or Zyla 4.2, Andor) and an LED light source (SPECTRA X Light Engine, Lumencor or X-Cite TURBO, Excelitas Technologies). A 20× objective lens (Plan Apo VC, Nikon) and filter sets (Ex: 480/40 nm, Dichroic: 505 nm, Em: 535/50 nm) were used for fluorescence imaging. Time-lapse images were obtained at 10–30 min intervals for a total of 360 min (or 10 min intervals for a total of 40 min in buffer exchange experiment at each FDP concentration) with an exposure time of 200 ms. The fluorescence images were analyzed using Fiji and custom-written macros. To precisely determine the peak area, uneven illumination was corrected by applying a flat-field correction to the images using a fluorescein solution.[64]

ACKNOWLEDGMENTS

We thank all members of our laboratory for helpful comments. We thank Y. Zhang and M. Sakuma for technical discussion. This work was supported in part by Grant-in-Aid for Scientific Research on Innovation Areas (JP18H04817, JP19H05380) from the Japan Society for the Promotion of Science (to Hiroshi Ueno); Platform Project for Supporting Drug Discovery and Life Science Research (Basis for Supporting Innovative Drug Discovery and Life Science Research [BINDS]) from AMED under Grant Number JP21am0101115 and by ImPACT Program of Council for Science, Technology, and Innovation, Japan Science and Technology Agency (to Hiroyuki Noji).

AUTHOR CONTRIBUTIONS

Hiroshi Ueno: Investigation; methodology; software; visualization. **Makoto Kato:** Investigation; methodology; software. **Yoshihiro Minagawa:** Methodology; software. **Yushi Hirose:** Investigation; methodology. **Hiroyuki Noji:** Conceptualization; supervision.

CONFLICT OF INTEREST

The authors declare no conflict of interest.

ORCID

Hiroshi Ueno https://orcid.org/0000-0001-5331-4335

REFERENCES

1. Cohen L, Walt DR. Single-molecule arrays for protein and nucleic acid analysis. Annu Rev Anal Chem. 2017;10, 345–363.
2. Zhang Y, Noji H. Digital bioassays: Theory, applications, and perspectives. Anal Chem. 2017;89:92–101.
3. Vogelstein B, Kinzler KW. Digital PCR. Proc Natl Acad Sci USA. 1999;96:9236–9241.
4. Agresti JJ, Antipov E, Abate AR, et al. Ultrahigh-throughput screening in drop-based microfluidics for directed evolution. Proc Natl Acad Sci USA. 2010;107:4004–4009.
5. Heyries KA, Tropini C, Vaninsberghe M, et al. Megapixel digital PCR. Nat Methods. 2011;8:649–651.
6. Ottesen EA, Hong JW, Quake SR, Leadbetter JR. Microfluidic digital PCR enables multigene analysis of individual environmental bacteria. Science. 2006;314:1464–1467.
7. Pekin D, Skhiri Y, Baret JC, et al. Quantitative and sensitive detection of rare mutations using droplet-based microfluidics. Lab Chip. 2011;11:2156–2166.
8. Shen F, Du W, Kreutz JE, Fok A, Ismagilov RF. Digital PCR on a SlipChip. Lab Chip. 2010;10:2666–2672.
9. Kim SH, Iwai S, Araki S, Sakakihara S, Iino R, Noji H. Large-scale femtoliter droplet array for digital counting of single biomolecules. Lab Chip. 2012;12:4986–4991.
10. Rissin DM, Kan CW, Campbell TG, et al. Single-molecule enzyme-linked immunosorbent assay detects serum proteins at subfemtomolar concentrations. Nat Biotechnol. 2010;28:595–599.
11. Akama K, Iwanaga N, Yamawaki K, et al. Wash- and amplification-free digital immunoassay based on single-particle motion analysis. ACS Nano. 2019;13:13116–13126.
12. Akama K, Noji H. Multiplexed homogeneous digital immunoassay based on single-particle motion analysis. Lab Chip. 2020;20:2113–2121.

13. Rissin DM, Walt DR. Digital concentration readout of single enzyme molecules using femtoliter arrays and Poisson statistics. Nano Lett. 2006;6:520–523.
14. Sakakihara S, Araki S, Iino R, Noji H. A single-molecule enzymatic assay in a directly accessible femtoliter droplet array. Lab Chip. 2010;10:3355–3362.
15. Yelleswarapu V, Buser JR, Haber M, Baron J, Inapuri E, Issadore D. Mobile platform for rapid sub-picogram-per-milliliter, multiplexed, digital droplet detection of proteins. Proc Natl Acad Sci USA. 2019;116:4489–4495.
16. Liu W, Chen D, Du W, Nichols KP, Ismagilov RF. SlipChip for immunoassays in nanoliter volumes. Anal Chem. 2010;82:3276–3282.
17. Soga N, Ota A, Nakajima K, Watanabe R, Ueno H, Noji H. Monodisperse liposomes with femtoliter volume enable quantitative digital bioassays of membrane transporters and cell-free gene expression. ACS Nano. 2020;14:11700–11711.
18. Gorris HH, Rissin DM, Walt DR. Stochastic inhibitor release and binding from single-enzyme molecules. Proc Natl Acad Sci USA. 2007;104:17680–17685.
19. Rondelez Y, Tresset G, Tabata KV, et al. Microfabricated arrays of femtoliter chambers allow single molecule enzymology. Nat Biotechnol. 2005;23:361–365.
20. Mogalisetti P, Gorris HH, Rojek MJ, Walt DR. Elucidating the relationship between substrate and inhibitor binding to the active sites of tetrameric beta-galactosidase. Chem Sci. 2014;5:4467–4473.
21. Liebherr RB, Renner M, Gorris HH. A single molecule perspective on the functional diversity of in vitro evolved beta-glucuronidase. J Am Chem Soc. 2014;136:5949–5955.
22. Ehrl BN, Liebherr RB, Gorris HH. Single molecule kinetics of horseradish peroxidase exposed in large arrays of femtoliter-sized fused silica chambers. Analyst. 2013;138:4260–4265.
23. Obayashi Y, Iino R, Noji H. A single-molecule digital enzyme assay using alkaline phosphatase with a cumarin-based fluorogenic substrate. Analyst. 2015;140:5065–5073.
24. Minagawa Y, Ueno H, Tabata KV, Noji H. Mobile imaging platform for digital influenza virus counting. Lab Chip. 2019;19:2678–2687.
25. Tabata KV, Minagawa Y, Kawaguchi Y, et al. Antibody-free digital influenza virus counting based on neuraminidase activity. Sci Rep. 2019;9:1067.
26. Watanabe R, Soga N, Fujita D, et al. Arrayed lipid bilayer chambers allow single-molecule analysis of membrane transporter activity. Nat Commun. 2014;5:4519.
27. Zhang Y, Minagawa Y, Kizoe H, et al. Accurate high-throughput screening based on digital protein synthesis in a massively parallel femtoliter droplet array. Sci Adv. 2019;5:eaav8185.
28. Coleman JE. Structure and mechanism of alkaline phosphatase. Annu Rev Biophys Biomol Struct. 1992;21:441–483.
29. Carr C, O'neill BE, Hochhalter CB, Strong MJ, Ware ML. Biomarkers of pineal region tumors: A review. Ochsner J. 2019;19:26–31.
30. Hammerich KH, Donahue TF, Rosner IL, et al. Alkaline phosphatase velocity predicts overall survival and bone metastasis in patients with castration-resistant prostate cancer. Urol Oncol. 2017;35:460.
31. Lee J, Bubar CT, Moon HG, et al. Measuring bone biomarker alkaline phosphatase with wafer-scale nanowell array electrodes. ACS Sens. 2018;3:2709–2715.
32. Pu N, Gao S, Xu Y, et al. Alkaline phosphatase-to-albumin ratio as a prognostic indicator in pancreatic ductal adenocarcinoma after curative resection. J Cancer. 2017;8:3362–3370.
33. Xiao Y, Lu J, Chang W, et al. Dynamic serum alkaline phosphatase is an indicator of overall survival in pancreatic cancer. BMC Cancer. 2019;19:785.
34. Zhu Y, Ye DW. Prostate cancer: Alkaline phosphatase velocity in nonmetastatic CRPC. Nat Rev Urol. 2014;11:666–667.
35. Sakamoto S, Komatsu T, Watanabe R, et al. Multiplexed single-molecule enzyme activity analysis for counting disease-related proteins in biological samples. Sci Adv. 2020;6:eaay0888.
36. Jiang Y, Li X, Walt DR. Single-molecule analysis determines isozymes of human alkaline phosphatase in serum. Angew Chem Int Ed Engl. 2020;132:2–8.
37. Craig DB, Arriaga EA, Wong JCY, Lu H, Dovichi NJ. Studies on single alkaline phosphatase molecules: Reaction rate and activation energy of a reaction catalyzed by a single molecule and the effect of thermal denaturation - the death of an enzyme. J Am Chem Soc. 1996;118:5245–5253.
38. Polakowski R, Craig DB, Skelley A, Dovichi NJ. Single molecules of highly purified bacterial alkaline phosphatase have identical activity. J Am Chem Soc. 2000;122:4853–4855.
39. Masaike T, Koyama-Horibe F, Oiwa K, Yoshida M, Nishizaka T. Cooperative three-step motions in catalytic subunits of F(1)-ATPase correlate with 80 degrees and 40 degrees substep rotations. Nat Struct Mol Biol. 2008;15:1326–1333.
40. Nishizaka T, Oiwa K, Noji H, et al. Chemomechanical coupling in F1-ATPase revealed by simultaneous observation of nucleotide kinetics and rotation. Nat Struct Mol Biol. 2004;11:142–148.
41. Mandecki W, Shallcross MA, Sowadski J, Tomazic-Allen S. Mutagenesis of conserved residues within the active site of *Escherichia coli* alkaline phosphatase yields enzymes with increased kcat. Protein Eng. 1991;4:801–804.
42. O'Brien PJ, Herschlag D. Alkaline phosphatase revisited: Hydrolysis of alkyl phosphates. Biochemistry. 2002;41:3207–3225.
43. Stec B, Holtz KM, Kantrowitz ER. A revised mechanism for the alkaline phosphatase reaction involving three metal ions. J Mol Biol. 2000;299:1303–1311.
44. Boulanger RR Jr, Kantrowitz ER. Characterization of a monomeric *Escherichia coli* alkaline phosphatase formed upon a single amino acid substitution. J Biol Chem. 2003;278:23497–23501.
45. McCall KA, Huang C, Fierke CA. Function and mechanism of zinc metalloenzymes. J Nutr. 2000;130:1437S–1446S.
46. Sone M, Kishigami S, Yoshihisa T, Ito K. Roles of disulfide bonds in bacterial alkaline phosphatase. J Biol Chem. 1997;272:6174–6178.
47. Tuckey C, Asahara H, Zhou Y, Chong S. Protein synthesis using a reconstituted cell-free system. Curr Protoc Mol Biol. 2014;108:1–22.
48. Shimizu Y, Inoue A, Tomari Y, et al. Cell-free translation reconstituted with purified components. Nat Biotechnol. 2001;19:751–755.
49. Anderson RA, Bosron WF, Kennedy FS, Vallee BL. Role of magnesium in *Escherichia coli* alkaline phosphatase. Proc Natl Acad Sci USA. 1975;72:2989–2993.

50. Derman AI, Beckwith J. *Escherichia coli* alkaline phosphatase localized to the cytoplasm slowly acquires enzymatic activity in cells whose growth has been suspended: A caution for gene fusion studies. J Bacteriol. 1995;177:3764–3770.
51. Zhang L, Buchet R, Azzar G. Distinct structure and activity recoveries reveal differences in metal binding between mammalian and *Escherichia coli* alkaline phosphatases. Biochem J. 2005;392:407–415.
52. Bloch W, Schlesinger MJ. Kinetics of substrate hydrolysis by molecular variants of *Escherichia coli* alkaline phosphatase. J Biol Chem. 1974;249:1760–1768.
53. Bradshaw RA, Cancedda F, Ericsson LH, et al. Amino acid sequence of *Escherichia coli* alkaline phosphatase. Proc Natl Acad Sci U S A. 1981;78:3473–3477.
54. Nakata A, Shinagawa H, Shima H. Alkaline phosphatase isozyme conversion by cell-free extract of *Escherichia coli*. FEBS Lett. 1984;175:343–348.
55. Nesmeyanova MA, Motlokh OB, Kolot MN, Kulaev IS. Multiple forms of alkaline phosphatase from *Escherichia coli* cells with repressed and derepressed biosynthesis of the enzyme. J Bacteriol. 1981;146:453–459.
56. Lazdunski M, Petitclerc C, Chappelet D, Lazdunski C. Flip-flop mechanisms in enzymology. A model: The alkaline phosphatase of *Escherichia coli*. Eur J Biochem. 1971;20:124–139.
57. Chappelet-Tordo D, Fosset M, Iwatsubo M, Gache C, Lazdunski M. Intestinal alkaline phosphatase. Catalytic properties and half of the sites reactivity. Biochemistry. 1974;13:1788–1795.
58. Orhanovic S, Pavela-Vrancic M. Dimer asymmetry and the catalytic cycle of alkaline phosphatase from *Escherichia coli*. Eur J Biochem. 2003;270:4356–4364.
59. Hoylaerts MF, Manes T, Millan JL. Mammalian alkaline phosphatases are allosteric enzymes. J Biol Chem. 1997;272:22781–22787.
60. Fan DP, Schlesinger MJ, Torriani A, Barrett KJ, Levinthal C. Isolation and characterization of complementation products of *Escherichia coli* alkaline phosphatase. J Mol Biol. 1966;15:32–48.
61. Hehir MJ, Murphy JE, Kantrowitz ER. Characterization of heterodimeric alkaline phosphatases from *Escherichia coli*: An investigation of intragenic complementation. J Mol Biol. 2000;304:645–656.
62. Schlesinger MJ, Levinthal C. Hybrid protein formation of *E. coli* alkaline phosphatase leading to in vitro complementation. J Mol Biol. 1963;7:1–12.
63. Pedregosa F, Varoquaux G, Gramfort A, et al. Scikit-learn: Machine learning in python. J Machine Learn Res. 2011;12:2825–2830.
64. Zwier JM, Van Rooij GJ, Hofstraat JW, Brakenhoff GJ. Image calibration in fluorescence microscopy. J Microsc. 2004;216:15–24.

SUPPORTING INFORMATION

Additional supporting information may be found online in the Supporting Information section at the end of this article.

How to cite this article: Ueno H, Kato M, Minagawa Y, Hirose Y, Noji H. Elucidation and control of low and high active populations of alkaline phosphatase molecules for quantitative digital bioassay. Protein Science. 2021;30:1628–1639. https://doi.org/10.1002/pro.4102